Journal of Fluorine Chemistry 205 (2018) 43–48

Contents lists available at ScienceDirect

Journal of Fluorine Chemistry

journal homepage: www.elsevier.com/locate/fluor

Short Communication

Decomposition of CoF_3 during battery electrode processing

Wei Li[a], Henri Groult[a], Olaf J. Borkiewicz[b], Damien Dambournet[a,c,*]

[a] Sorbonne Universités, UPMC Univ Paris 06, CNRS UMR 8234, Laboratoire PHENIX, 4 place Jussieu, F-75005 Paris, France
[b] X-ray Science Division, Advanced Photon Source, Argonne National Laboratory, 9700 South Cass Avenue, Argonne, Illinois 60439, United States
[c] Réseau sur le Stockage Electrochimique de l'Energie (RS2E), FR CNRS 3459, 80039 Amiens, France

ARTICLE INFO

Keywords:
Corundum
Rutile
ReO3
Pair distribution function
Li-ion batteries

ABSTRACT

Metal fluorides are potential candidates as electrode materials for rechargeable batteries. During the electrode fabrication, however, thermal treatments can cause decomposition of thermally instable compounds. Here, we showed that during the electrode processing of CoF_3, the carbon and PVDF additives act as a protective layer that prevents CoF_3 to readily decompose into CoF_2 (rutile). We found that instead, it decomposes into an intermediate phase with a corundum like structure featuring Co vacancies, *i.e.*, $Co_{1.26}^{II}Co_{0.16}^{III}\square_{0.58}F_3$ where □ represents the vacancies. The structural analysis was possible owing to the use of the pair distribution function.

PACS(optional, as per journal): 75.40.-s; 71.20.LP

1. Introduction

Since the pioneer work of Poizot et al. [1] on the use of binary transition metal oxide as conversion materials for lithium-ion batteries, a large number of compounds have been reported to undergo such a multi-electronic redox reaction [2]. Particularly, extended studies have been related to the use of transition metal fluorides including FeF_3, TiF_3, VF_3 and CoF_3 [3–6].

High valence metal fluorides such as CoF_3 can decompose into binary fluoride with the release of molecular fluorine gas which make them potential solid fluorinating agent [7]. The thermal decomposition path of CoF_3, however, largely depends on the operating conditions [8]. Traces of humidity can promote the decomposition of CoF_3 according to:

$$2CoF_3 + H_2O \rightarrow 2CoF_2 + 2HF + \tfrac{1}{2}O_2 \quad (1)$$

Hence, CoF_3 should be handled in dry conditions to prevent decomposition [6].

The preparation of battery electrodes which are composite of electroactive material, carbon and a polymeric matrix comprises several steps [9]. The mixing of electroactive material, carbon with polyvinylidene fluoride (PVDF) binder is usually performed with N-Methyl-2-pyrrolidone (NMP) solvent. The slurry is then casted onto a current collector. The solvent is evaporated at low temperature, *i.e.*, 60–70 °C below the flash point (96 °C) of NMP. To remove traces of humidity, a final heat treatment is usually performed at a temperature of around 105 °C. All these steps can alter the structure/composition of the electroactive material. Here, we investigated the impact of these steps on the structure/composition of CoF_3 electrode by means of high-energy total scattering data. We showed that the presence of carbon and binder enables to limit the decomposition of CoF_3. By structural analysis of the electrode, we discovered a new phase, intermediate between CoF_3 and CoF_2, whose structure was solved using a rhombohedral cell isostructural to the corundum type structure with Co vacancies. This work points to the necessity to careful handling when dealing with certain metal fluorides.

2. Results and discussion

To investigate the decomposition mechanism of CoF_3 during electrode processing, we considered three types of samples that are the pristine CoF_3 (handled in a dry glove box), CoF_3 treated at 70 °C under air to mimic the solvent removal step and the electrode. It should be noted that the preparation of the electrode was performed using hand-milling which does not impact the crystal structure of the material. High intensity synchrotron based X-ray (λ = 0.2128 Å) scattering measurements was performed at the Advanced Photon Source. For convenience, the data were re-scaled in two-theta at the wavelength of

* Corresponding author at: Sorbonne Universités, UPMC Univ Paris 06, CNRS UMR 8234, Laboratoire PHENIX, 4 place Jussieu, Paris, F-75005, France.
E-mail address: damien.dambournet@upmc.fr (D. Dambournet).

https://doi.org/10.1016/j.jfluchem.2017.11.012
Received 8 September 2017; Received in revised form 27 November 2017; Accepted 28 November 2017
Available online 29 November 2017

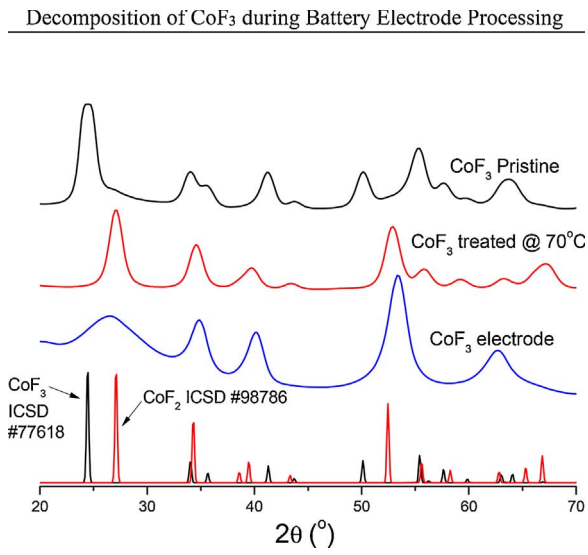

Fig. 1. High-energy X-ray diffraction patterns of pristine CoF_3 (black), CoF_3 treated at 70 °C under ambient atmosphere (red) and electrode (blue). Reference XRD patterns of CoF_2 and CoF_3. (For interpretation of the references to colour in this figure legend, the reader is referred to the web version of this article.)

copper λ_{Cu} = 1.54 Å (Fig. 1). The X-ray diffraction pattern of the pristine CoF_3 can be indexed using a rhombohedral *R*-3*c* cell [10]. We also noted a small amount of CoF_2 impurity [11]. After a thermal treatment at 70 °C under ambient atmosphere, CoF_3 readily converts to CoF_2. The electrode XRD pattern, however, differs from both CoF_3 and CoF_2 and could not be indexed using crystallographic database [12]. Moreover, the Bragg peaks showed broad lines that complexify the structural determination by conventional Rietveld analysis.

To better understand the composition and structural changes associated with the decomposition process of CoF_3, we used the pair distribution function (PDF), G(*r*), which was obtained by Fourier transformed high-energy X-ray total scattering data. By providing real-space structural representation, PDF enables to obtain detailed information at the local to long-range order particularly suited to study disordered/nanostructured/amorphous compounds [13]. PDFs of the pristine CoF_3, CoF_2 (CoF_3 treated at 70 °C under ambient atmosphere) and the electrode are gathered in Fig. 2 with selected *r*-region characteristic of short-range, *i.e.*, $1 \leq r \leq 6$ Å, and intermediate/long-range orders, *i.e.*, $r > 4$ Å. PDF represents a histogram of all atom–atom distances within the sample. The first peak located at around 2 Å corresponds to Co-F bonds. The position of the Co-F pair can be obtained by Gaussian fitting of the first peak yielding 2.04 Å for CoF_2 and 1.94 Å for CoF_3. In the electrode, the first peak is centered at 2.03 Å which is close to that found in CoF_2 and is therefore related to Co^{II}-F distances indicating that CoF_3 was reduced during the electrode fabrication. The second peak at around 3.1 Å is close to Co–Co pairs found in the rutile CoF_2 and arises from edge-shared CoF_6 octahedra (label A, $d_{Co\text{-}Co}$ = 3.17 Å). This peak is absent in CoF_3 which features only corner-shared CoF_6 octahedra with $d_{Co\text{-}Co}$ = 3.6–3.7 Å (label B). Note that the rutile phase presents both edge- and corner-shared CoF_6 octahedra as revealed by the presence of the two sets of distances. At $r > 4$ Å, the PDF features of the electrode differ from those found in CoF_2 and CoF_3 indicating a different structural arrangement in agreement with XRD data.

To identify the structure stabilized during the electrode fabrication, we attempted to fit the PDF data using a real-space refinement [14]. First, we refined the PDF of pristine CoF_3 and CoF_2 (obtained by CoF_3 treated at @70 °C) starting from previously reported structures [10,11]. Fig. 3 presents the refined PDFs with reliability factors R_w that attest the goodness of the fits. Following X-ray diffraction data, the PDF of the pristine CoF_3 was refined using two-phase models based on CoF_3 (space group *R*-3*c*) and CoF_2 (space group P4/2mnm). The amount of CoF_2 and CoF_3 within the pristine was 25 and 75at%, respectively. Selected structural parameters extracted from the refinement are gathered in Table 1 and are in good agreement with previously reported structures [10,11].

To fit the PDF of the electrode, we used different structural models particularly structures that shared common structural features. Notably, it is known that the corundum and rutile are structurally related [15]. According to the X-ray diffraction pattern in Fig. 2, the rutile CoF_2 phase seems to be present with a broad Bragg peak at around 26–27 2θ(°) which can be indexed with the (110) line of the tetragonal cell. Hence, we included it in the fit. Finally, the best fit (Fig. 3**)** was obtained using a corundum-type phase Co_2F_3. Moreover, the determination of the PDF scattering domain (sp parameter in the PDFGui software) yielded 8 nm which explained the broadness of the Bragg peaks. Table 2 gathered the structural parameters of the corundum phase obtained from the PDF refinement. The refinement of the Co (12c) rate occupancy indicates the presence of Co vacancies. Based on the general composition, the refined atomic occupancy yields $Co_{1.26}{}^{II}Co_{0.16}{}^{III}\square_{0.58}F_3$.

Here, we showed that CoF_3 decomposes to CoF_2 via an intermediate phase derived from the corundum type structure. The structural representations of the three phases CoF_2, $Co_{1.26}{}^{II}Co_{0.16}{}^{III}\square_{0.58}F_3$ and CoF_3 are presented in Fig. 4. Further works should be carried out to better understand the decomposition mechanism of CoF_3 along with phase transformation path from ReO_3, corundum to rutile type structures.

The as prepared electrode was cycled in glavanostatic mode versus metallic lithium. Fig. 5 shows the galvanostatic curves obtained under 50 mAg^{-1} with LP30 as the electrolyte. The theoretical capacity of $Co_{1.26}{}^{II}Co_{0.16}{}^{III}\square_{0.58}F_3$ is 572 mAh g^{-1}. Upon discharge, a pseudo plateau region was observed at an average potential of 1.65 V yielding a capacity around 550 mAh g^{-1} which is close to the theoretical capacity. Moreover, the average potential is 350 mV higher than the one display by CoF_2 showing a slight variation of the insertion voltage between the two structures. The full discharge yielded around 1230 mAh g^{-1} which can be assigned to the electrolyte decomposition. After the first charge, the capacity decreased to 505 mAh g^{-1} which suggest that the conversion reaction is almost reversible. Finally, after the second cycle, the capacity further decreased to 410 mAh g^{-1} which might be due to the inability to reach the trivalent state of cobalt in a reversible manner [6].

3. Conclusion

In this work, we reported on the structural analysis of an electrode made of CoF_3. Based on high-energy X-ray data, we showed that CoF_3 decomposes during the electrode processing into a new structure/composition. Using the pair distribution function, we discovered that this structure corresponds to a defective corundum phase featuring Co vacancies, *i.e.*, $Co_{1.26}{}^{II}Co_{0.16}{}^{III}\square_{0.58}F_3$. Hence, the decomposition of CoF_3 (ReO_3) toward CoF_2 occurred via the corundum structure.

4. Experimental

4.1. Materials preparation and electrochemical measurements

Thermal treatment of CoF_3 pristine powder was conducted at 70 °C